Journal of Oil Palm Research
DOI: https://doi.org/10.21894/jopr.2025.0022

STUDY OF THE ANATOMICAL STRUCTURE ALONG THE OIL PALM FRUIT BUNCH STALK AND ITS IMPACT ON CUTTING PRESSURE

AZHAR ARIFF[1]; CHONG WU YI[1]*; HARITH AHMAD[1]; MOHAMMAD FAISAL ISMAIL[1]; WAN RUSYDIAH WAN RUSIK[2]; BATRISYIA AHMAD NAZRI[3]; AMIRUL AL HAFIZ ABDUL HAMID[4]; HARIKRISHNA KULAVEERASINGAM[2]; MOHAMMAD ZULFAHMI MOHAMMAD YUSOFF[4] and MOHAMMAD SHIRAZ ARIS[4]

ABSTRACT

The variation in anatomical characteristics of 16-year-old African oil palm fruit bunch stalk and its effect on mechanical cutting were investigated. Variations in vascular bundle (VB) density, VB size, parenchyma tissue area ratio, and total cross-sectional area along the length of the fruit bunch stalk were analysed. The correlation between cutting pressure and the corresponding anatomical structures was then established. Results show that vascular bundle density decreases from the proximal to distal positions of the fruit bunch stalk, whereas total cross-sectional area and vascular bundle size increase from the proximal to distal positions. The variation of the parenchyma tissue area ratio does not vary significantly. Multivariate regression analysis shows a positive correlation between VB density and VB size with cutting pressure ($R^2 = 0.741$), with the influence of VB density on cutting pressure being much larger than the effect of VB size. From the results of complete fruit bunch stalk cutting, it is found that the required cutting pressure is lowest when cutting at the middle section of the stalk, halfway between the stalk ring and the fruit bunch rachis.

Keywords: anatomical structure, cutting resistance, fruit bunch stalk, oil palm, vascular bundle.

Received: 16 July 2024; **Accepted:** 2 January 2025; **Published online:** 28 March 2025.

INTRODUCTION

The oil palm is one of the most valuable crops in the agriculture industry. A total of 5.67 million hectares of land in Malaysia will be utilised for oil palm plantations in 2022 [Malaysia Palm Oil Board (MPOB), 2022]. Globally, the palm oil industry had a market size of USD70.44 billion in 2023 and is forecast to reach close to USD100.00 billion per year by 2030 (Grand View Research, 2024). Palm oil is ubiquitous - used to make a range of everyday products such as foods, cosmetics, soaps, lubricants and biodiesel (Basiron & Weng, 2004). There has also been extensive research on the use of palm oil by-products to produce furniture, animal feed, paper and biomass fuel to eliminate waste from the palm oil industry (Basiron & Weng, 2004; Suhaily *et al.*, 2012).

The common type of oil palm cultivated in Southeast Asia is the species *Elaeis guineensis*. It is a monocotyledon and its stems generally comprise parenchyma tissue (PT) and vascular bundle (VB) fibres (Parthasarathy & Klotz, 1976). Monocotyledons and their VBs appear to be distributed randomly across the transverse section of the trunk/stem. However, research has since shown that the VBs actually follow a

[1] Photonics Research Centre,
Science Faculty Universiti Malaya,
50603 Kuala Lumpur, Malaysia.

[2] SD Guthrie Berhad, Level 3,
Main Block, Plantation Tower
No. 2, Jalan PJU 1A/7, Ara Damansara,
47301 Petaling Jaya, Selangor, Malaysia.

[3] SD Guthrie Research Sdn. Bhd.,
KM10 Jalan Banting-Kelanang,
42700 Banting, Selangor, Malaysia.

[4] SD Guthrie Research Sdn. Bhd.,
R&D Centre – Carey Island,
Lot 2664, Jalan Pulau Carey,
42960 Pulau Carey, Kuala Langat, Selangor, Malaysia.

* *Corresponding author e-mail: wuyi@um.edu.my*

systematic pathway through the stems of the plants (Zimmermann & Tomlinson, 1972). VBs of monocotyledons function as the primary supporting structure and the transport vessels of the plant. They consist of the xylem and the phloem, which transport water and nutrients respectively (Corley & Tinker, 2016; Dickison, 2000; Tomlinson, 1961). PTs on the other hand are the site for metabolic processes like glucose conversion into starch as well as its storage (Bakar *et al.*, 2008; Lim & Gan, 2005). Crucially, VBs can be visibly distinguished from the surrounding PT.

Though efforts have been put into the mechanisation of oil palm harvesting (Hao & Lai, 2024; Qun, 2023) the harvesting of the oil palm fruit bunch stalks (FBS) has relied solely on manual labour using chisels and sickles, which is labour intensive and physically demanding. To improve the harvesting efficiency of oil palm FBS, Jelani *et al.* (1998) investigated the effect of cutter design, cutting angle and frond age on cutting force using conventional sickles and a mechanical claw. Similarly, Intara *et al.* (2013) investigated the physical and mechanical properties of oil palm FBS and fronds for use in designing mechanical pruners and harvesters. It has been shared by harvesters that the difficulty of cutting FBS depends on which section along the FBS is being cut. Therefore, the variation in the FBS's anatomical structure from the base (proximal) to the top (distal) of the FBS may be the reason for the difference in cutting difficulty.

Darwis *et al.* (2013) examined the correlation between VB distribution and the mechanical properties of the African oil palm (*E. guineensis*) trunks (OPT). Their results showed that the modulus of rupture (MoR) and the shearing resistance parallel to the grain of the OPT increased as the VB density increased from bark to pith, indicating a directly proportional relationship between VB density and these mechanical properties. In the same study, however, they also found that the trunk taken from the top segment of the OPT has lower mechanical strength compared with the bottom segments despite having more VBs. The authors attributed this observation to the age of the trunk section, which is younger at the top segment than at the bottom segment.

Fathi and Frühwald (2014) investigated the effect of VB dimensions and distribution on the mechanical properties of coconut palm (*Cocos nucifera*) trunks. The obtained results showed that the mechanical strength of a coconut trunk decreases as the VB density decreases from the bark to the pith section. A similar study on date palm (*Phoenix dactylifera*) trunks, on the other hand, yielded the opposite result. Fathi *et al.* (2017) discovered that the tensile strength and modulus of elasticity of trunk samples increased with decreasing VB density and the number of VBs from bark to pith of the date palm, which is the opposite correlation to their initial study on coconut palm.

According to studies on the vasculature of monocotyledonous plants, VBs indeed have a greater influence on the mechanical properties of the stem/stalk/trunk than the surrounding tissue. In previous studies, however, shearing resistance perpendicular to grain and its relationship to VB density, have not been studied. Furthermore, there are no systematic studies on this relationship with oil palm stalk. Since oil palm bunch harvesting involves the cutting of a large volume of FBS, this information is essential in improving the harvesting efficiency of oil palm FBS.

In this article, the variations in cross-sectional anatomical properties *i.e.*, VB density, VB size, PT area ratio and total cross-sectional area along the proximal to distal sections of the FBS are determined. The effect of the anatomical properties on the cutting pressure is analysed. Multivariate regression analysis is used to establish the relationships between the anatomical properties and cutting pressure.

MATERIALS AND METHODS

The type of oil palm used in this study is cultivated by SD Guthrie Bhd. (Malaysia). It is of the species *E. guineensis* of the Deli *dura* x AVROS *pisifera* variant. All FBS samples used in this study were taken from different palm plants within the same plantation group of 16 years old. Furthermore, the FBS samples are of the same stage of ripeness corresponding to the age of harvesting to reduce the differences in development stages between different FBS samples. Freshly harvested FBS are transported to the lab and processed on the same day.

The region of stalk cut during harvesting is along the stalk peduncle, between the stalk ring and the fruit bunch rachis. So anatomical structure and force measurements are made within this region. The experiment is divided into two parts. In the first part, the anatomical feature measurements and mechanical cutting are conducted on small, consistently dimensioned sub-sections of the stalk cross-section. This method avoids additional forces *e.g.*, the wedging effect and surface contact friction during the cutting process, isolating the cutting interaction between the blade and FBS's anatomical features. This section of the experiment will be referred to as "sub-section cutting". The second part involves the analysis of anatomical variations along the oil palm FBS and the study of the cutting force required during actual harvesting. This section will be referred to as "complete FBS cutting".

Sample Preparation

For the preparation of sub-section stalk samples, an FBS was first cut into five sections along its proximal to distal length with the most proximal position assigned as No. 1 and the most distal position assigned as No. 5. The most proximal position is between 2 and 4 cm from the stalk ring and each subsequent position is 3 cm apart. Each cross-section was further divided into sub-sections of approximately 2×1×1 cm as shown in *Figure 1c*. The sub-sections at the periphery of the cross-section have their rinds removed to eliminate their contribution to cutting resistance. A total of 21 sub-sections were prepared and analysed. In addition, a separate set of 23 sub-sections samples were prepared for validation purposes.

On the other hand, a total of 11 FBS were analysed for their anatomical variation along the stalk length. Cutting pressure measurement was also carried out on 7 of the FBSs. Each FBS was assigned a letter from A to K. Similarly, the cross-sections were numbered according to their positions along the FBS. The most proximal position was assigned as No. 1 and the most distal position was assigned the highest number according to the stalk length. Each section was approximately equidistant from its neighbouring sections. Stalks E and H were divided into seven and six sections, respectively, as these two stalks are longer in length. The remaining nine stalks were divided into three sections. An example of an FBS cut into three transverse cross-sections along the length of the FBS is shown in *Figure 2*.

In addition, the moisture content of FBS at different sections along the FBS stalks has been measured by comparing their weight before and after drying at 105°C for 24 hr (Mandang *et al.*, 2018). The average moisture content is measured to be 81 ± 1%. Therefore, the contribution of moisture content to the variation in cutting characteristics along the FBS stalk is not significant.

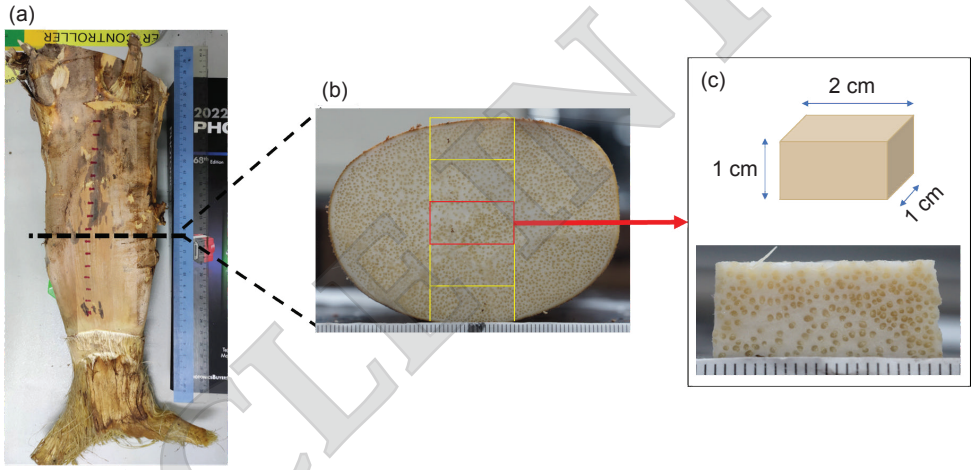

Figure 1. Division of cross-sections into smaller sub-sections for cutting. (a) Whole FBS, (b) cross-section of FBS and (c) sub-section with dimensions of approximately 2x1x1 cm.

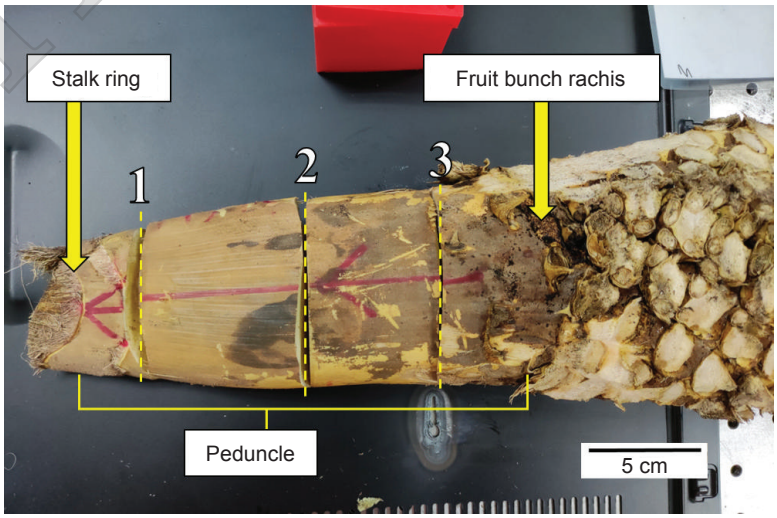

Figure 2. Stalk B is cut into three sections.

Image Analysis

Cross-section image analysis of small sub-sections was carried out using image processing software (ImageJ) and its features were measured manually. An example of a sub-section image analysed can be seen in *Figure 1c*. Three variables were measured for the sub-section image analysis which are the VB density, VB size and PT area ratio along with their corresponding uncertainties.

For the analysis of the complete FBS cross-section, an image of the entire cross-section was first captured. Then, close-up images of different parts of the cross-section were taken for image analysis. VB density, VB size and PT area ratio were then measured using ImageJ. All images were taken using a digital single lens translucent camera (Sony A77) with appropriate lighting. The images were first adjusted to improve the contrast between the VBs and the surrounding PTs as shown in *Figure 3a* and *3b*. The image was then converted to 8-bit greyscale and subsequently to binary image via binary thresholding as shown in *Figure 3c* and *3d*, respectively. The conversion to a binary image must fulfil the following two conditions: (1) Distinguishable VB silhouettes with minimal VB overlap, and (2) comparable VB silhouette size to source.

A region with clearly distinguishable VBs is required for accurate counting. An example of the region with distinguishable VBs is enclosed in a square shown in *Figure 3d*. *Figure 3e* shows the zoomed-in image of the enclosed square. Noise reduction was conducted followed by watershedding to produce an image with more well-defined VBs as shown in *Figure 3f*. The processed image is then compared with the initial, unedited cross-sectional image (*Figure 3a*) via visual inspection and manual VB size measurements. Any mismatch detected between the features in the two images is manually corrected (*e.g.*, by drawing lines to separate VBs that were not watershed by software, filling holes in the VBs for an accurate measurement of VB size and manual removal of noise elements). A blue boarder around a feature indicates that the software identifies it as a particle as shown in *Figure 3g*. This process is repeated until the software accurately identifies all appropriate elements.

VB density was obtained by dividing the number of VBs counted by the area being analysed. The uncertainty in VB density is based on the estimated number of miscounted VBs. The value of the uncertainty was obtained by comparing the processed image with the actual image of a specific cross-section and identifying VBs that were missed or split. The average VB density uncertainty was measured to be around ± 3.5%.

The VB size was calculated by the software at the step shown in *Figure 3*. To verify the accuracy

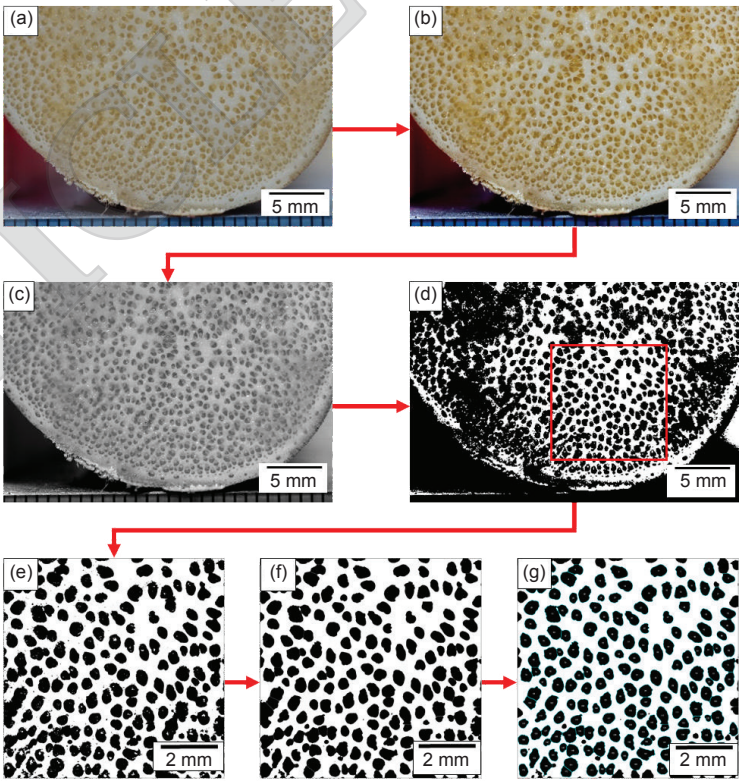

Figure 3. Image processing steps and the resultant images. (a) Original image, (b) contrast adjusted image, (c) conversion to 8-bit greyscale, (d) binary thresholding, (e) high distinguishability region, (f) noise reduction, watershedding, manual correction, (g) particle counting and size measurements.

of VB size, 30 selected VBs from the contrast adjusted image (*Figure 3*) were manually measured and compared with the VB sizes obtained from software analysis. The average VB size was obtained by averaging all measured VB sizes. The measurement uncertainty in average VB size is approximately ± 6 %.

Finally, the PT area ratio is derived from both VB density and VB size and was calculated using the following Equation (1):

$$PT\ area\ ratio\ (\%) = (1 - [average\ VB\ size \times average\ VB\ density]) \times 100\% \quad (1)$$

Cutting Force Measurement

Cutting was carried out using a cut force measurement apparatus. The apparatus is set up according to the Universal Testing Machine reported by Intara *et al.* (2013). A schematic diagram and a photo of the apparatus are shown in *Figure 4*. It consists of the stalk cutter, an aluminium frame, a weighing scale and a jack. The stalk cutter uses blades with a height and thickness of 25.00 and 0.65 mm, respectively. The blade edge is tapered at an angle of 17° with a tapering length of 2.00 mm. A blade edge width of 0.30 mm was used to calculate the cutting pressure. The stalk cutter frame that holds the blade is constructed of solid wood and is guided by aluminium rods and slide bearings. It is set up to apply a force perpendicular to the cutting surface of the blade.

An aluminium frame is erected over the stalk cutter and a jack is placed between the frame and the top of the stalk cutter. To measure the weight exerted during cutting, a weighing scale was placed under the stalk cutter. The weighing scale has a sensitivity of 50 g.

Typically, cutting force is measured in the form of a specific cutting force (Ahmad *et al.*, 2020; Boydaş *et al.*, 2019; Jelani *et al.*, 1998; Zhang *et al.*, 2018) which is analogous to shear force. The Equation (2) for specific cutting force (SCF) is,

$$SCF = \frac{F_{max}}{A} \quad (2)$$

where F_{max} is the maximum force exerted during the cutting and A is the cross-sectional area of the cut plane.

However, it is more relevant to calculate the pressure required to cut through the stalk using the relationship in Equation (3):

$$Pressure\ (N.mm^{-2}) = \frac{Weight\ measured\ (kg) \times g\ (10\ m.s^{-2})}{Blade\ edge\ width\ (0.3\ mm) \times Stalk\text{-}blade\ contact\ length\ (mm)} \quad (3)$$

When cutting sub-section samples, the samples are placed flat on the cutter bed with the fibres oriented perpendicular to the cutter blade. The cut force and its corresponding cross-sectional anatomy for each sub-section cut were measured at the mid-section of the sample.

When cutting the complete FBS stalk, the orientation of the fibres relative to the blade is similar to sub-section cutting. The FBS stalk is first cut into smaller sections for ease of handling and placed flat on the cutter bed. Due to the irregular shape of the stalk segments, wedges were placed underneath the stalk segment to avoid tilting during cutting. The force is measured at the instance when the blade is fully embedded into the FBS. This position is selected

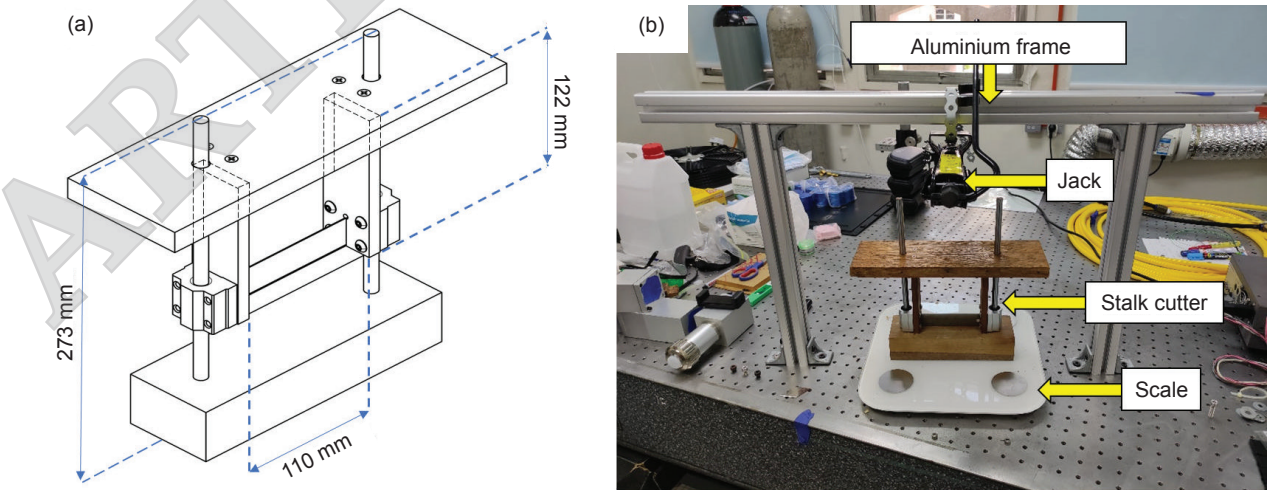

Figure 4. (a) Schematic drawing of stem cutter and (b) photo of the complete setup.

primarily to minimise the wedging effect or friction on the blade that occurs as it further embeds into the stalk's tissue. This method also standardises the measurement process across all samples. Calculating pressure normalises the force exerted on a unit of area, which takes into account the contribution of varying sample width to the cutting force required to cut through. This is especially important when cutting complete FBSs as their widths vary along the cutting direction.

RESULTS AND DISCUSSION

Vascular Bundle Distribution Across the FBS Cross-Section

Figure 5 shows three cross-sections taken from three different proximal to distal positions along stalk D. Using ImageJ to mark the radial distance, the distribution of VBs was qualitatively assessed. It is found that the VB distribution changes along the length of the FBS. The proximal section (No. 1) has the highest density of VBs at the centre of the FBS as shown in *Figure 5a* and *5b*. A reduction in VB density begins at 0.4 R to 0.7 R of the FBS (R is the radial distance from the centre to the edge of the FBS cross-section) before increasing again towards the circumference of the FBS. The middle section (No. 2) of the FBS and its close-up image are shown in *Figure 5c* and *5d*, respectively. It shows an evenly distributed VB density over the entire cross-section. The distal section (No. 3) of the FBS and its close-up image are shown in *Figure 5e* and *5f*. Similar to the proximal section, the distal section has a denser distribution of VBs at the centre of the cross-section. This distribution extends to approximately 0.7 R. Beyond this radial position, the VB density drastically reduces before increasing again towards the circumference of the FBS. In all of the three positions, the cross-sections show a radial symmetry for VB distribution.

Sub-section Cutting

A total of 21 sub-section samples have been used in this study. It was found that the VB density ranges from 97-187 cm^{-2}, while the VB size ranges from 0.00175-0.00347 cm^2. The PT area ratio, which is a product of VB density and VB size, ranges from 64.2%-77.3%. It is observed that higher VB density corresponds to smaller VB size and *vice versa*. The minimum cutting pressure measured was 12.0 $N.mm^{-2}$, which corresponds to the lowest VB density. Whereas the maximum cutting pressure of 22.9 $N.mm^{-2}$ was measured for the sample with the second highest VB density. The trends between cutting pressure and VB size as well as the PT area ratio are not obvious. However, the correlation between anatomical features and cutting pressure requires a more detailed statistical analysis to be established. As the cutting pressure may depend on more than one anatomical parameter, multivariate regression analysis was used to investigate their correlations.

Correlation Between VB Density, VB Size and Cutting Pressure

Multivariate regression analysis using the Generalised Reduced Gradient Method was carried out to investigate the correlation between the anatomical features and cutting pressure. Two anatomical features, namely VB density and VB size, are used as variables. Since the PT area ratio is the

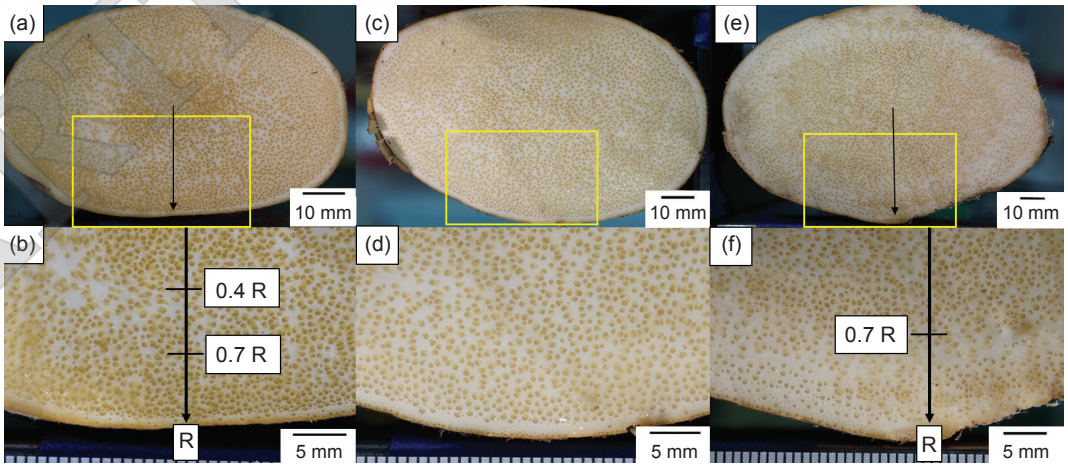

Figure 5. Cross-sections of stalk F (a) at position No. 1 with x1.7 magnification; (b) at position No. 1 with x10.3 magnification; (c) at position No. 3 with x1.3 magnification; (d) at position No. 3 with x11.4 magnification; (e) at position No. 5 with x1 magnification; and (f) at position No. 5 with x11.6 magnification. The yellow box in the upper images highlights the regions that correspond to the bottom images. The black arrows represent an estimation of the radius, R, of the stalk cross-sections.

product of VB density and VB size, an individual term for the PT area ratio is not considered. An equation that weighs the contributions of VB density and VB size towards cutting pressure is postulated as Equation (4):

$$P = R + C_{\rho}\rho^{\alpha} + C_{A}A^{\beta} \quad (4)$$

where, P is the pressure, C_{ρ} and C_{A} is the scaling coefficients, ρ is the VB density, A is the VB size, R is the lump parameters, α and β are the power scaling of VB density and VB size respectively.

From regression analysis, the coefficients are determined to be R = -0.4637, C_{ρ} = 0.1051 N, C_{A} = 74.7465 N.mm^{-1}, α = 1 and β = 0.5. The contribution of VB size to cutting pressure is found to be much smaller compared to VB density. Also, cutting pressure scales by the square root of VB size. The lump parameter, R was found to be close to 0. This indicates that additional systemic contributors to the cutting force are insignificant. These coefficients are used to calculate the cutting pressure required for different VB densities and VB sizes. *Figure 6* shows the comparison between the calculated cutting pressures and their corresponding experimental values and a validation plot using a separate dataset to test the regression equation. The linear regression (R-squared) is 0.7413 with a gradient of close to 1, which shows good agreement between the calculated and experimentally measured cutting pressure.

The validation plot is obtained by processing a separate dataset consisting of 23 sub-section samples using the regression model. The gradient of the validation plot is close to that of the original regression dataset, which is 1.0726 *vs* 1.0021 (a difference of 7%), with both datasets intercepting near the origin.

The results in *Figure 6* show that VB density is the primary contributor to cutting pressure. Although, there are no prior reports on the correlation between cutting pressure on the VB density of oil palm FBS, previous studies on OPT have shown a positive correlation between VB density and modulus of rupture (MOR), which is analogous to shear resistance perpendicular to grain (Darwis *et al.*, 2013). Darwis *et al.* (2013) reported a MoR on OPT samples ranging from 5-20 N.mm^{-2} following a procedure similar to sub-section cutting. This shows that mechanical cutting forces for OPT and FBS are similar. Oil palm VBs, compared with PTs, have a higher amount of α-cellulose – the most stable and polymerised form of cellulose (Abe *et al.*, 2013) which make up the thick-walled, fibrous sclerenchyma cells that surround the VBs. An increased Young's modulus and tensile strength are known to be attributed to increased cellulose content (McLaughlin & Tait, 1980). Thus, the combination of both great cell wall properties and high vascular bundle density would result in high mechanical properties of the overall plant tissue (Gibson, 2012).

VBs of the oil palm act like rebar in concrete by bounding the surrounding parenchyma tissue matrix more firmly, adding to the embedded material's shear resistance and overall mechanical properties (Dickison, 2000). Additionally, fibres going through a material impede the propagation of cracks within the material under stress. The greater the density of fibres the greater the reduction in breaking or cracking in the material/tissue, keeping it intact while the tensile strength of the uncut fibres resists the tissues separation (Moon *et al.*, 2011; Wilson *et al.*, 2013). In addition, the number of VBs that the blade edge comes into contact with at any instance during the cutting process is directly proportional to the VB density and FBS width. Therefore, with increasing VB

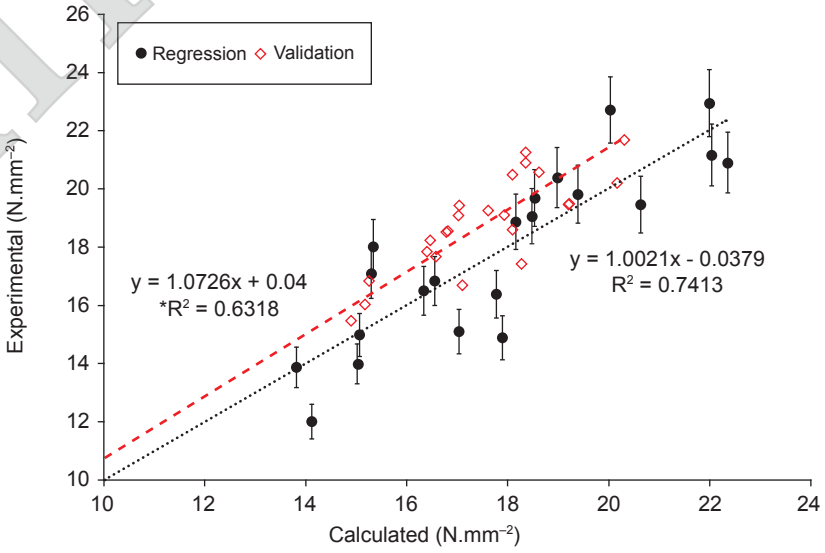

Figure 6. Sub-section cutting regression plot and validation plot.

density, the blade has to cut more VB fibres over the same width, which would increase cutting difficulty.

Complete FBS Cutting

Cutting force dynamics through stalk. *Figure 7* shows three different cutting force profiles that were observed when cutting through complete FBS. A smooth cutting process is shown in *Figure 7a*, where the cut force increases at the beginning of the cutting as the blade enters the stalk, and reaches a maximum around the middle section, before decreasing towards the end. The change in measured cut force corresponds to the stalk width profile along the cutting direction.

While a smooth cutting process is desirable, there were instances where in some cutting processes the blade is "caught" by the stalk tissue because of the wedging effect which is a countering force that acts against the separating force exerted by the blade (Libretexts, 2021). Coupled with friction between the stalk cross-section surface and the blade, these effects provide a formidable resistance to cutting which requires additional force to overcome. *Figure 7b* shows a sudden increase in cutting force around 26 mm into the stalk followed by a sudden decrease at 33 mm. This can be attributed to transitions between static and kinetic friction, also referred to as stick-slip motion experienced by the blade against the tissue of the FBS at low cutting speeds and under high friction (Berman *et al*., 1996; Martins *et al*., 1990).

In addition, there are also cuttings where the cutting force beyond the mid-section of the FBS remains high and does not return to zero at the end of the cutting process as seen in *Figure 7c*. This can be attributed to the deformation of the blade as it travels through the stalk tissue, which was visually observed. The deformation causes a gap between the blade and the surface of the stem cutter base. This results in the FBS rind remaining intact in the gaps between the blade and the base, while the frame of the blade holder is already pressing on the base.

Based on the analysis of the cutting force dynamics, the stick-slip motion and blade deformation occur after cutting through the centre of the FBS. Therefore, the measurement of cutting force was standardised and made at the instance when the blade is fully embedded (25 mm into the FBS). This coincides with the centre region of the FBS, where the maximum cut force was measured for most of the FBS samples.

Anatomy and pressure results. A total of 11 stalks were analysed for their anatomical variations from proximal to distal positions, while cutting pressure was measured in seven stalks. The total cross-sectional area for all FBS samples increases considerably from the proximal to distal positions. Increasing by 19% from positions No. 1 to No. 2 and a further 15% from positions No. 2 to No. 3. The average PT area ratio increases from proximal to distal positions by 4% across all FBSs. The variation is relatively small due to the simultaneous decrease

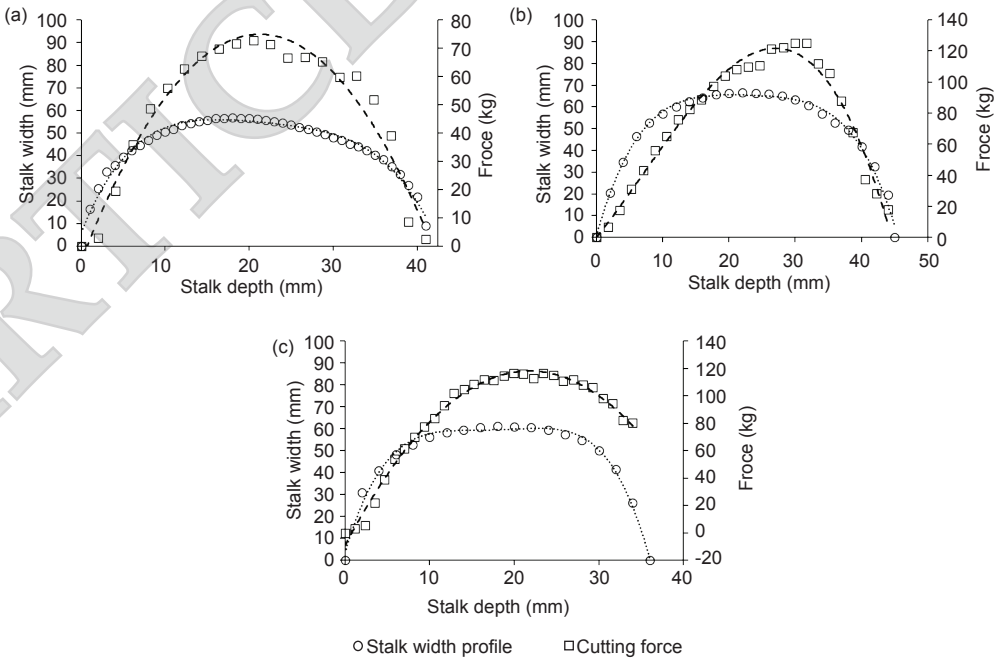

Figure 7. Changes in force at a given cut depth for three force-measured cut samples. (a) A relatively ideal cut with minimal sudden fluctuations in cut force, and a close to zero end cut force, (b) cut force spikes up after approximately 26 mm and cut force drops at 33 mm, and (c) cut force remains high at the end of the stalk.

in VB density and increase in VB size along the FBS. This falls within the measurement uncertainty. Coupled with the fact that the PT area ratio is a product of VB density and VB size, subsequent analysis will focus on the variation of VB density and VB size.

Figure 8a and *8b* shows the VB density and VB size values of each stalk at their corresponding positions as well as their average normalised values for each position. It can be seen that VB density trends downward from proximal to distal, while VB size increases from proximal to distal. For both VB density and VB size, a larger increase (decrease) was observed from positions No. 1 to No. 2 compared to from positions No. 2 to No. 3. On average, VB density decreases by 18% from positions No. 1 to No. 2 and a further 7% from positions No. 2 to No. 3. While VB size increases by 16% from position No. 1 to No. 2 and a further 1% from position No. 2 to No. 3.

The general path of the VBs of monocots along the stem is well understood. VBs spiral upward along the stem, then bend and divide into the leaves, inflorescence, or form bridges with other VBs (Corley & Tinker, 2016; Dickison, 2000). In the current study, the stalk surface is bare in the sense that it lacks leaves or other organs, until it reaches the fruits and spikelets. This limits VB branching at the proximal sections of the FBS to the interconnecting bridges between neighbouring VBs. Thus, up to the fruits, it can be postulated that the number of VBs remains relatively constant, only multiplying upon closer proximity to the fruits of the stalk. The total number of VBs measured across all samples on average increases by 15% from proximal to distal positions. However, VB density still reduces from proximal to distal due to the more significant increase in total cross-sectional area. On the other hand, there are no reports that explain the variation in VB sizes along the same FBS.

Figure 8c shows the measured cutting pressure of each stalk at their corresponding positions as well as their average values for each position. Based on the results, cutting through the complete FBS at the middle section requires the least force. The cutting pressure varies between 39.87 and 63.68 $N.mm^{-2}$, 39.12 and 49.65 $N.mm^{-2}$ and 42.46 and 55.19 $N.mm^{-2}$ for position No. 1, No. 2 and No. 3, respectively and their corresponding average cutting pressure are 54.08, 43.62 and 49.56 $N.mm^{-2}$, respectively.

In summary, results show that cutting through the middle section of the FBS requires about 10% less force compared to cutting close to the fruit bunch rachis. Given that position No. 1 of the FBS is usually covered by the fronds and the fact that the FBS size increases towards the fruit bunch rachis, cutting the stalk at its lowest exposed position will require the least amount of force. Although a 10% reduction in required cut force does not appear substantial, cumulative cutting of a large number of stalks during actual harvesting operations amounts to significant savings in energy expenditure. This will be increasingly essential when the harvesting process becomes further mechanised in the estates,

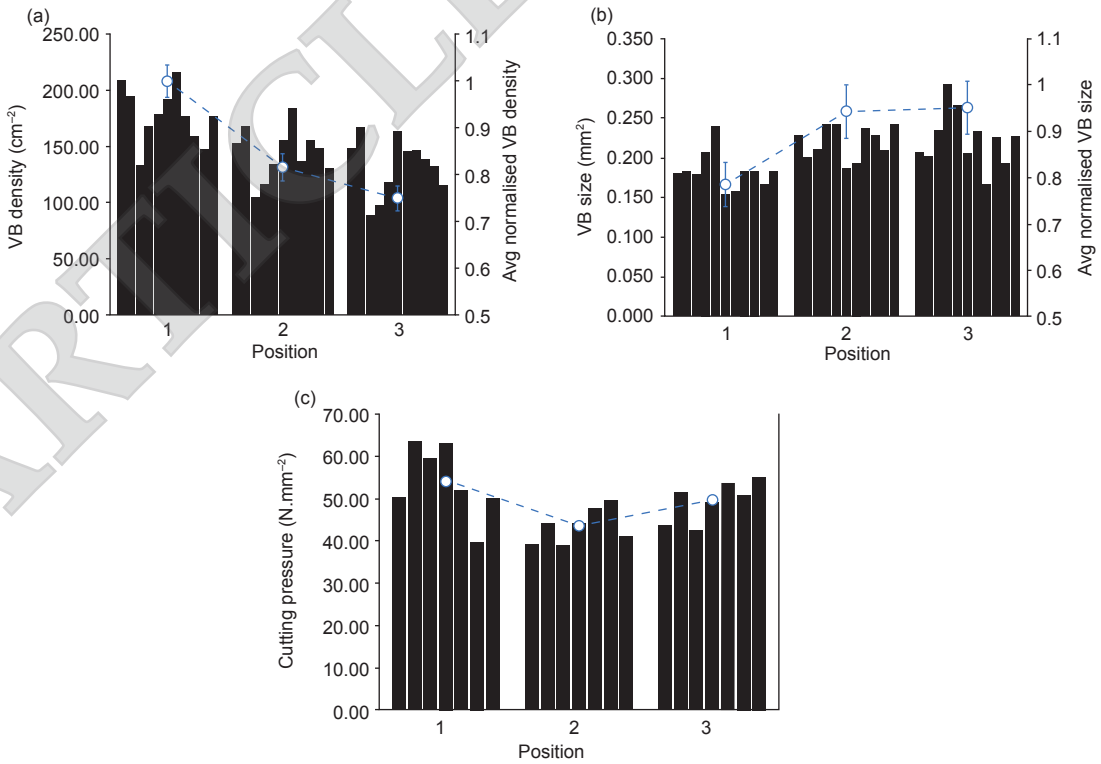

Figure 8. (a) VB density, (b) VB size and (c) cutting pressure for different positions along the FBS. Each column represents a specific stalk, with the left most column being stalk A ascending to stalk K. The marker plot represents the average values for each position.

where energy consumption has to be strictly managed and optimised.

Note that the cutting pressure required to cut through complete FBS is more than double that for sub-section cutting. This can be attributed to the wedging effect and friction between the stalk cross-section surface and the blade as discussed above. Larger cross-sections introduce a larger friction and greater wedging effect on the blade, while also causing more blade deformation. To verify if the correlation between VB density, VB size and cutting pressure established in sub-section cutting still applies, a comparison between the measured cut pressure and the calculated values is made in the next section.

Comparisons with sub-section cutting. The relationship between cutting pressure and FBS anatomy was analysed using the same equation and coefficients determined from sub-section cutting. *Figure 9* compares the measured cutting pressure with the calculated values. A similar linear trend between experimental and calculated cutting pressure is still observed. In addition, although quantitatively separating the contributions of the material's strength and frictional effects has been difficult (Williams, 1998), the measured cutting pressure for complete FBS cuts is found to be 2.5 times higher than that required for sub-section cutting, with an average measured cutting pressure of 46.87 N.mm^{-2} and the average calculated cutting pressure of 17.85 N.mm^{-2}.

Table 1 shows the multivariate regression analysis of both sub-section and complete FBS cutting. The table shows that sub-section cutting produces a better correlation between FBS cross-sectional anatomy and cutting pressure as evident by the better R^2 and significance, *F*-value. The *P*-values of the coefficients for both sub-sections and complete FBS cutting confirm that VB density is the most significant contributor to cutting pressure since it is the only coefficient with a *P*-value less than 0.05.

CONCLUSION

Cross-sectional anatomical structure analysis was conducted on oil palm FBS and its influence on cutting pressure was investigated. An equation relating VB density, VB size and cutting pressure is established. When cutting sub-sections of the FBS, results show that VB density has the most significant contribution towards cutting pressure. In the analysis of the anatomical structure of complete FBS, VB density was found to decrease from proximal to distal positions by an average of 25%, while VB size and PT area ratio increased from proximal to distal positions of the FBS by 17% and 4% respectively. When cutting through complete FBS, cutting pressure was found to be the least at the middle sections of the FBS, half-way between the stalk ring and fruit bunch rachis. Cutting through the complete FBS introduces additional resistances due to the wedging effect and stalk-blade surface contact friction. For oil palm FBS, specifically this results in 2.5 times increase in required cutting pressure when compared to sub-section cutting.

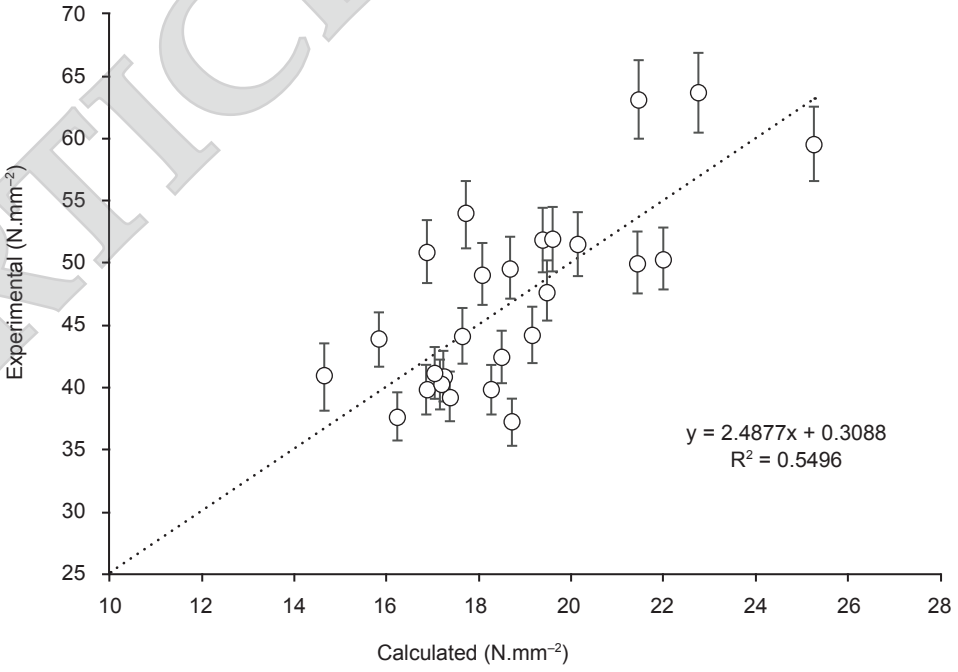

Figure 9. Plot of experiment versus predicted cutting pressure using the equation and coefficients from sub-section cutting.

TABLE 1. STATISTICAL RESULTS FOR MULTIVARIATE REGRESSION ANALYSIS OF SUB-SECTION AND COMPLETE FBS CUTTING

Sub-section cutting						
Item	**Coefficients**	***P*-value**	**R^2**	**Standard error**	**Sample size**	**Significance F**
Intercept	-0.4637	0.9585	0.7413	1.621	21	$5x10^{-6}$
VB density (cm^{-2})	0.1051	0.00011				
VB size (cm^2)	74.7465	0.5594				
Complete FBS cutting						
Item	**Coefficients**	***P*-value**	**R^2**	**Standard error**	**Sample size**	**Significance F**
Intercept	41.01088	0.112391	0.604609	4.950623	25	$4x10^{-5}$
VB density (cm^{-2})	0.19013	0.005156				
VB size (cm^2)	-486.075	0.209861				

ACKNOWLEDGEMENT

This project was supported by SD Guthrie Research Sdn. Bhd., (formerly known as Sime Darby Plantations Research) grant (PV032–2021) and Universiti Malaya IDIG grant (PPSI–2020–CLUSTER–IDIG06).

Disclosure statement

No potential conflict of interest was reported by the author(s).

REFERENCES

Abe, H., Murata, Y., Kubo, S., Watanabe, K., Tanaka, R., Sulaiman, O., Hashim, R., Ramle, S. F. M., Zhang, C., Noshiro, S., & Mori, Y. (2013). Estimation of the ratio of vascular bundles to parenchyma tissue in oil palm trunks using NIR spectroscopy. *BioResources*, *8*(2), 1573–1581. https://doi.org/10.15376/biores.8.2.1573-1581

Ahmad, M. R., Jamaludin, N., Jelani, A. R., Bakri, A., & Shuib, A. R. (2020). The effect of design parameters on the force and energy requirement for cutting oil palm fronds using magnetic force. *Jurnal Teknologi*, *82*(4), 141–150. https://doi.org/10.11113/jt.v82.14236

Bakar, E. S., Sahri, M. H., & H, P. S. (2008). Anatomical characteristics and utilization of oil palm wood. In *The formation of wood in tropical forest trees: A challenge from the perspective of functional wood anatomy* (pp. 161–178). Penerbit Universiti Putra Malaysia.

Basiron, Y., & Weng, C. K. (2004). The oil palm and its sustainability. *Journal of Oil Palm Research*, 16(1), 1–10.

Berman, A. D., Ducker, W. A., & Israelachvili, J. N. (1996). Origin and characterization of different stick−slip friction mechanisms. *Langmuir*, *12*(19), 4559–4563. https://doi.org/10.1021/la950896z

Boydaş, M. G., Çomakli, M., Sayinci, B., & Kara, M. (2019). Effects of moisture content, internode region, and oblique angle on the mechanical properties of sainfoin stem. *Turkish Journal of Agriculture and Forestry*, *43*(2), 254–263. https://doi.org/10.3906/tar-1802-32

Corley, R. H. V., & Tinker, P. B. (2016). *The oil palm* (5th ed.). Wiley Blackwell.

Darwis, A., Nurrochmat, D. R., Massijaya, M. Y., Nugroho, N., Alamsyah, E. M., Bahtiar, E. T., & Safe`i, R. (2013). Vascular bundle distribution effect on density and mechanical properties of oil palm trunk. *Asian Journal of Plant Sciences*, *12*(5), 208–213. https://doi.org/10.3923/ajps.2013.208.213

Dickison, W. C. (2000). *Integrative plant anatomy*. Academic Press.

Fathi, L., & Frühwald, A. (2014). The role of vascular bundles on the mechanical properties of coconut palm wood. *Wood Material Science and Engineering*, *9*(4), 214–223. https://doi.org/10.1080/17480272.2014.887774

Fathi, L., Bahmani, M., Saadatnia, M. A., & Poursartip, L. (2017). An investigation on anatomical and mechanical properties of vascular bundles in date palm. *Iranian Journal of Wood and Paper Industries*, *8*(1), 109–118.

Gibson, L. J. (2012). The hierarchical structure and mechanics of plant materials. *Journal of the Royal Society Interface*, *9*(76), 2749–2766. https://doi.org/10.1098/rsif.2012.0341

Grand View Research. (2024). *Palm oil market size, share & trends analysis report by nature (organic, conventional), by product (fractionated palm oil,*

crude palm oil), by end-use (pharmaceuticals, biofuel & energy), by region, and segment forecasts, 2024–2030. Grand View Research. https://www.grandviewresearch.com/industry-analysis/palm-oil-market

Hao, T. K., & Lai, N. S. (2024). Autonomous harvesting robot for oil palm plantation: A review. *Journal of Oil Palm Research*. https://doi.org/10.21894/jopr.2024.0008

Intara, Y. I., Mayulu, H., & Radite, P. A. S. (2013). Physical and mechanical properties of palm oil frond and stem bunch for developing pruner and harvester machinery design. *International Journal of Science and Engineering*, *4*(2), 69–74. https://doi.org/10.12777/ijse.4.2.69-74

Jelani, A. R., Ahmad, D., Hitam, A., Yahya, A., & Jamak, J. (1998). Force and energy requirements for cutting oil palm fronds. *Journal of Oil Palm Research*, *10*(2), 10–24.

Libretexts. (2021, July 28). *6.3: Wedges*. https://eng.libretexts.org/Bookshelves/Mechanical_Engineering/Mechanics_Map_(Moore_et_al.)/06%3A_Friction_and_Friction_Applications/6.03%3A_Wedges.

Lim, S., & Gan, K. (2005). Characteristics and utilization of oil palm stem. *Timber Technology Bulletin*, *25*, 139–258.

Malaysian Palm Oil Board (MPOB). (2022). *Overview of the Malaysian Oil Palm Industry 2022*. https://bepi.mpob.gov.my/images/overview/Overview2022.pdf.

Mandang, T., Sinambela, R., & Pandianuraga, N. R. (2018). Physical and mechanical characteristics of oil palm leaf and fruits bunch stalks for bio-mulching. *IOP Conference Series Earth and Environmental Science*, *196*(1), 012015. https://doi.org/10.1088/1755-1315/196/1/012015

Martins, J. A. C., Oden, J. T., & Simoes, F. M. F. (1990). A study of static and kinetic friction. *International Journal of Engineering Science*, *28*(1), 29–92. https://doi.org/10.1016/0020-7225(90)90014-A

McLaughlin, E. C., & Tait, R. A. (1980). Fracture mechanism of plant fibres. *Journal of Materials Science*, *15*(1), 89–95. https://doi.org/10.1007/bf00552431

Moon, R. J., Martini, A., Nairn, J., Simonsen, J., & Youngblood, J. (2011). Cellulose nanomaterials review: Structure, properties and nanocomposites. *Chemical Society Reviews*, *40*(7), 3941–3994. https://doi.org/10.1039/c0cs00108b

Parthasarathy, M. V., & Klotz, L. H. (1976). Palm "Wood" I. Anatomical aspects. *Wood Science and Technology*, *10*(3), 215–229. https://doi.org/10.1007/BF00355742

Qun, S. (2023). Analysis of the energy consumption of motorised circular saw when cutting oil palm frond. *Journal of Oil Palm Research*. https://doi.org/10.21894/jopr.2023.0063

Suhaily, S. S., Jawaid, M., Khalil, H. P. S. A., Mohamed, A. R., & Ibrahim, F. (2012). *A review of oil palm biocomposites for furniture design and applications: Potential and challenges*. *BioResources, 7*(3), 4400–4423. https://doi.org/10.15376/biores.7.3.4400-4423

Tomlinson, P. B. (1961). *Anatomy of the monocotyledons. Volume II.* Oxford.

Williams, J. G. (1998). Friction and plasticity effects in wedge splitting and cutting fracture tests. *Journal of Materials Science, 33*(19), 5351–5357. https://doi.org/10.1023/A:1004490015211

Wilson, E., Mohammadi, M., & Nairn, J. (2013). Crack propagation fracture toughness of several wood species. *Advances in Civil Engineering Materials, 2*(1), 316–327. https://doi.org/10.1520/ACEM20120045

Zhang, Y., Cui, Q., Li, H., Sun, D., & Hou, H. (2018). Effects of stem region, moisture content and blade oblique angle on mechanical cutting of millet stems. *INMATEH - Agricultural Engineering, 55*(2), 105–112.

Zimmermann, M. H., & Tomlinson, P. B. (1972). The vascular system of monocotyledonous stems. *Botanical Gazette*, *133*(2), 141–155. https://doi.org/10.1086/336628